Supporting Information

Cerium Oxide-Modified Pd Nanosheets Encapsulated by Red Blood Cell Membranes with High-Efficiency RONS Scavenging for Depression Treatment

Xinyan Hu, [a] Xianhua Zhang, [b] Gongxin Zhang, [a] Dongxu Cao, [a] Zichen Ye, [a] and Xiaolan Chen *[a]

[a] *State Key Laboratory for Physical Chemistry of Solid Surfaces, Collaborative Innovation Center of Chemistry for Energy Materials, National & Local Joint Engineering Research Center of Preparation Technology of Nanomaterials, College of Chemistry and Chemical Engineering, Xiamen University, Xiamen 361005, China.*

[b] *Department of Mental Health Research, Xiamen Xianyue Hospital, Xiamen 361012, China.*

*E-mail: chenxl@xmu.edu.cn (Xiaolan chen)

Table of contents

1. Experimental Section

1.1 Material Characterizations.

Ultraviolet–visible (UV-Vis) absorption spectra were recorded using UVmini-1280 Shimadzu Vis-spectrometer (Japan). The morphology images of nanomaterials were obtained using a transmission electron microscope (HRTEM, JEM-1400). Thermo ScientificTM TalosTM F200X Transmission Electron Microscope was employed to carry out the lattice, energy spectra, line scan, area scan and mapping image of Pd-CeO_2 NSs (PC). The X-ray diffraction (XRD) pattern for PC was obtained using a powder X-ray diffractometer (Smartlab-SE XRD). Malvern Zetasizer Nano ZSE was used to carry out the zeta potential and hydrodynamic size measurements of nanomaterials. Solution oxygen level was determined by Shanghai Lei-magnetic portable dissolved oxygen analyzer (JPBJ-608). The cell viability was determined by Enzyme-labeled Instrument (Infinite M200, TECAN). The electron spin-resonance spectroscopy (ESR) signals of •OH were characterized by Bruker EMX-10/12 electron paramagnetic resonance spectrometer. The X-ray photoelectron spectra (XPS) were performed on an X-ray photoelectron spectrometer (Thermo Fisher Scientific K-Alpha +). Confocal laser fluorescence microscopy was gained from Leica Microsystems (Shanghai) Trading Co., Ltd.

1.2 Biosafety Experiments.

Hemolytic test. Fresh mouse blood was centrifuged at 1600 rpm/min for 15 minutes, and the pellet was rinsed in PBS four times. A total of 7 mL of PBS and 1.5 mL of sediment were mixed to generate a stock solution. Twenty microliters of stock solution were added to one milliliter of the sample solution before being subjected to a 20-minute spin at 1000 rpm/min. Then the supernatant's absorbance at 540 nm was measured via an enzyme-labeled apparatus.

Hemolysis ratio (%) = $(A_s - A_n) / (A_p - A_n) \times 100\ \%$

A_s: Red blood cell stock solution was mixed with the material; A_n: Red blood cell stock solution was mixed with PBS; A_p: Red blood cell stock solution was mixed with H_2O.

Pharmacokinetics of PCR. Healthy C57BL/6J mice were injected 200 μL of PCR (1 mg/mL) via tail vein. Blood was collected from tail vein at 10 min, 40 min, 1.5 h, 2 h, 6 h, 8 h, 24 h, 48 h and 72 h, and Pd contents of these samples were assessed via ICP-MS following digestion with a HNO_3-H_2O_2 (3:1) solution.

The Metabolism of PCR. Mouse wastes (urine and feces) were collected for a seven day period, subsequently treated with an HNO_3-H_2O_2 (3:1) mixture, and analyzed via ICP-MS for their Pd contents.

The weight changes of the mice were recorded for one week.

1.3 Animal Behavior Tests

Male C57BL/6 mice were obtained from the Laboratory Animal Center of Xiamen University. Animal experiments strictly complied with the guidelines of Xiamen University Animal Management and Ethics Committee (XMULAC20200128 (the original number is XMULAC20200129)).

Sucrose preference test (SPR). On day one, every cage was supplied with 1 % sucrose solution for mouse. The subsequent day, all cages were transferred to fresh water and withheld food for 24 h. Following the postfast period, the sucrose concentration was elevated to 2%. After another 24 h, intake of this sweetened water was documented.

Forced swimming test (FST). Forced swimming test, an approach that simulated drowning, created a persistently stressful yet impotent scenario. Utilizing super maze animals behavoiral analysis software, we observed alteration of mouse mental state, as seen in initial frantic attempts to evade the tank's waters before utimately floating on the surface of water.

The elevated plus maze (EPM). The elevated plus maze was a configuration of cross-like apparatuses, composes of an open-arm section and an enclosed arm section. Intersecting at their midpoint was a center area. The elevated cross simulated human feelings of apprehension faced with the edge of a precipice. Mice' spirital status was represented via their immobility times in both the open and enclosed arms.

Open field test (OFT). Mice displayed spontaneous engagement and exploratory behavior within novel environments, and their spiritual status could be examined through their open field performance. We quantified mouse' spirit state via detailed observation of their immobility times at each zones (four corners, periphery and center) and their mobility path. It's crucial to note post-experiment cleanliness by wiping the arena with alcohol before test. Mice were positioned in the center of the experimental chamber and began recording promptly.

The tail suspension test (TST). Through tail fixation, mice' bodies were inverted. Mice in this condition instinctively experienced a desperate urge for escapism as well as a profound desire to halt struggling when faced with escape impossible. The spiritual status of mice was quantified via the measurement of their immobility time.

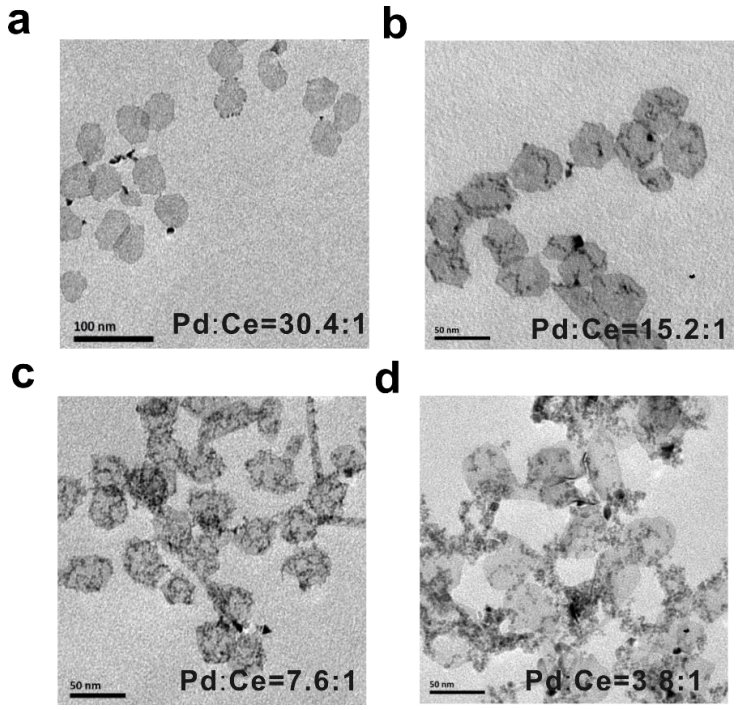

Figure S1. TEM images of PC with different Pd to Ce molar feeding ratio.

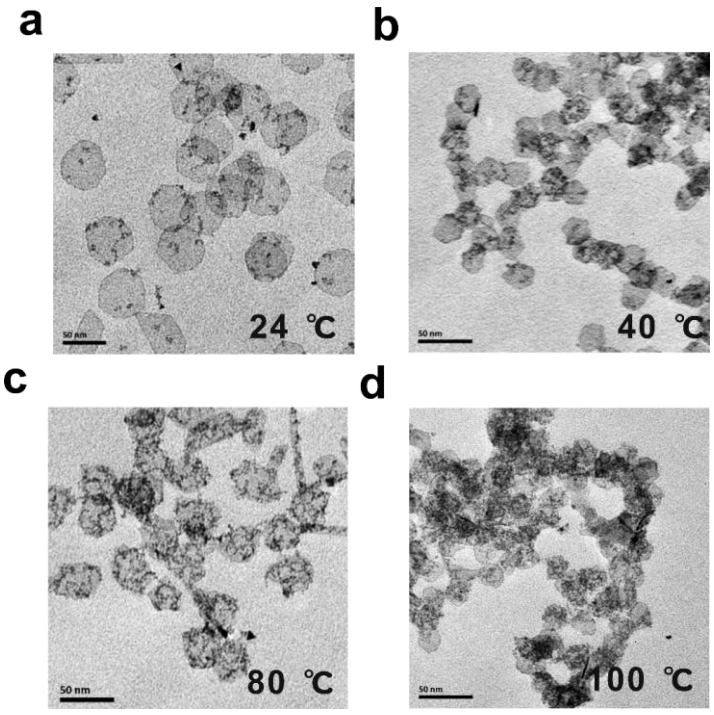

Figure S2. TEM images of PC with different reaction temperature.

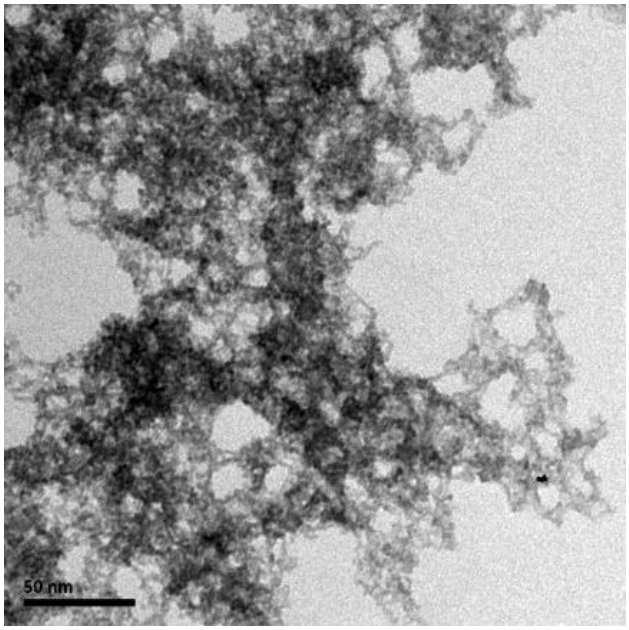

Figure S3. TEM image of CeO_2 nanoparticles.

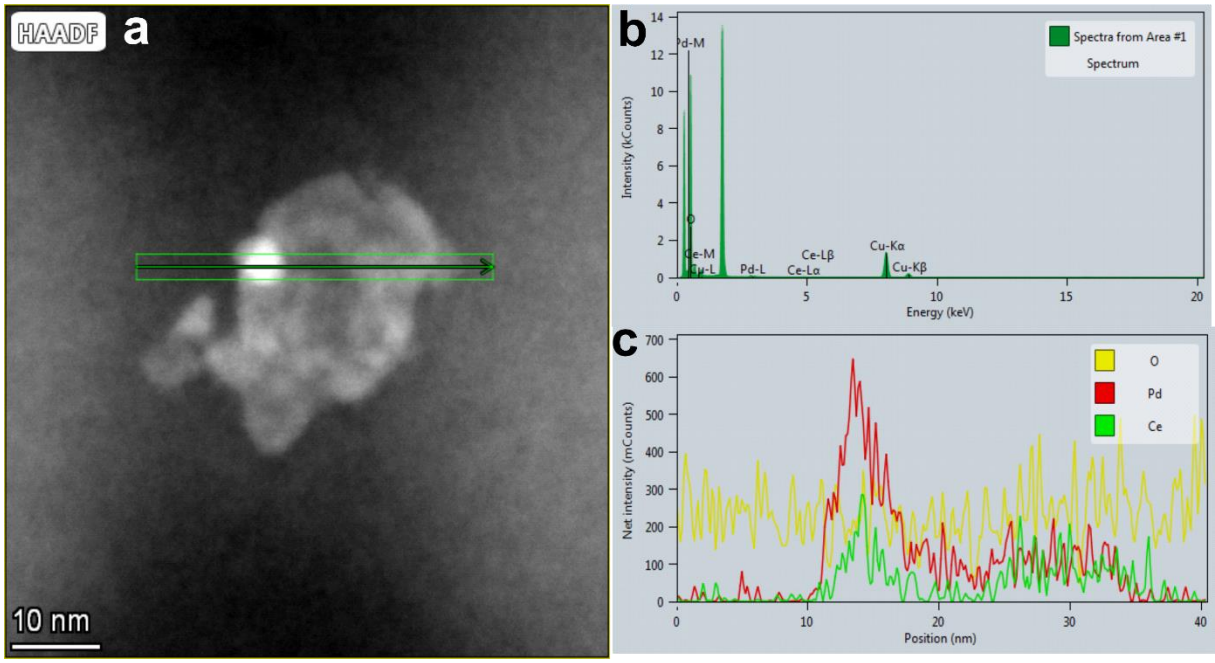

Figure S4. (a) HAADF image of PC. (b) EDX spectrum of PC. (c) Line-scan spectra of elemental Pd and Ce that were recorded along an edge-to-edge direction of the individual PC.

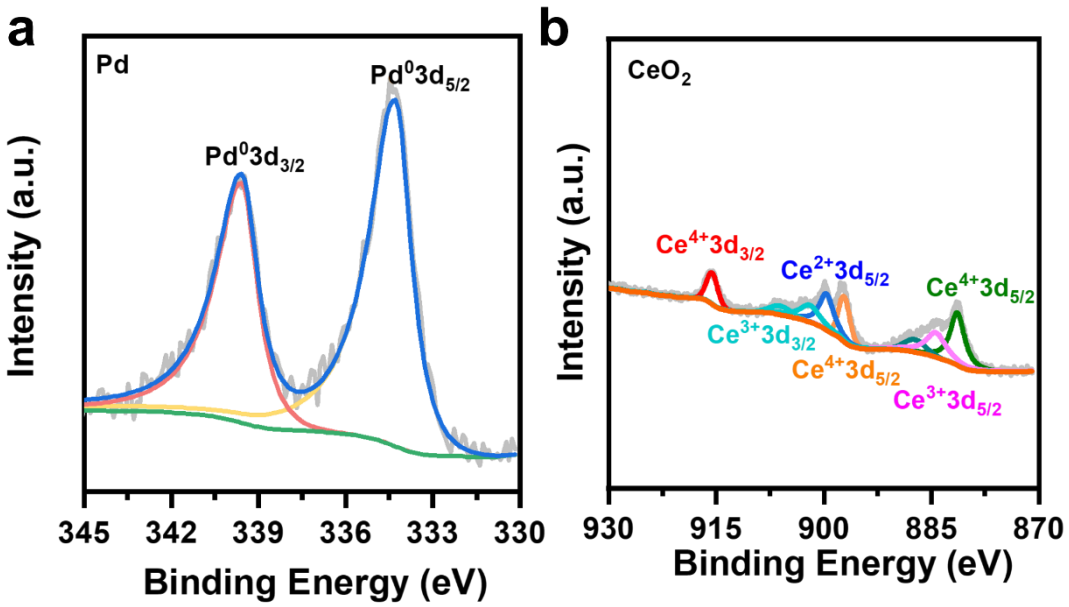

Figure S5. High-resolution XPS spectra of the Pd 3d ($Pd^0 3d_{5/2}$: 334.27 eV; $Pd^0 3d_{3/2}$: 339.56 eV) in Pd NSs (a), and Ce 3d ($Ce^{4+}3d_{3/2}$: 914.69 eV; $Ce^{4+}3d_{5/2}$: 896.45 eV, 887.16 eV, 880.46 eV; $Ce^{3+}3d_{3/2}$: 901.55 eV, 899.03 eV; $Ce^{3+}3d_{5/2}$: 883.48 eV) in CeO_2 NPs (b).

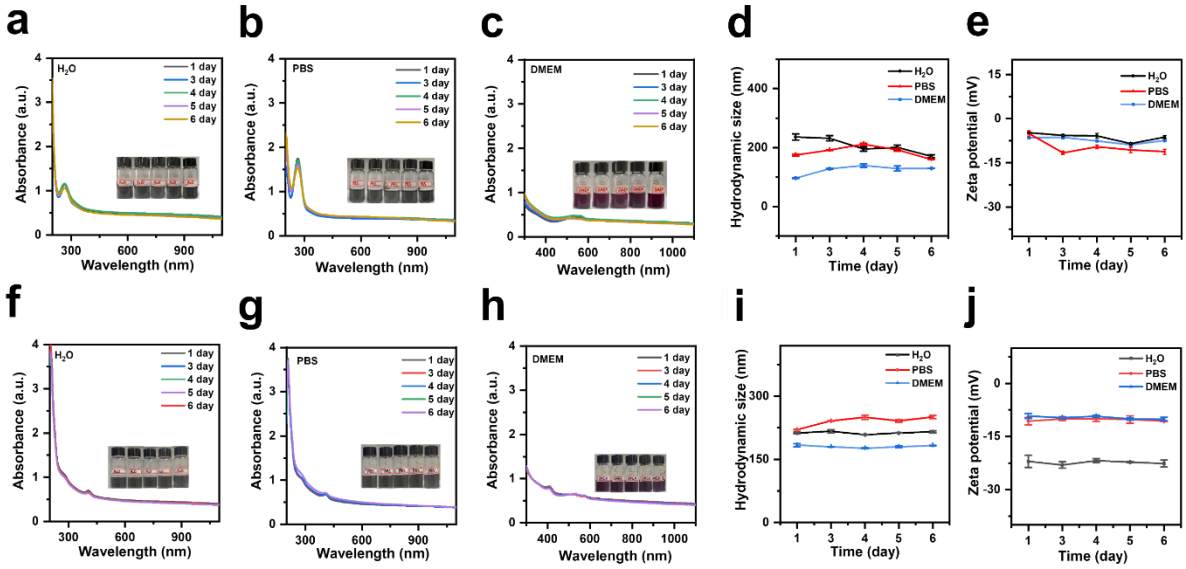

Figure S6. Stability of PC and PCR. UV-Vis-NIR spectra, size and zeta potential changes of PC (a-e) and PCR (f-j) dispersed in H_2O, PBS and DMEM media at 4 °C for one week, respectively.

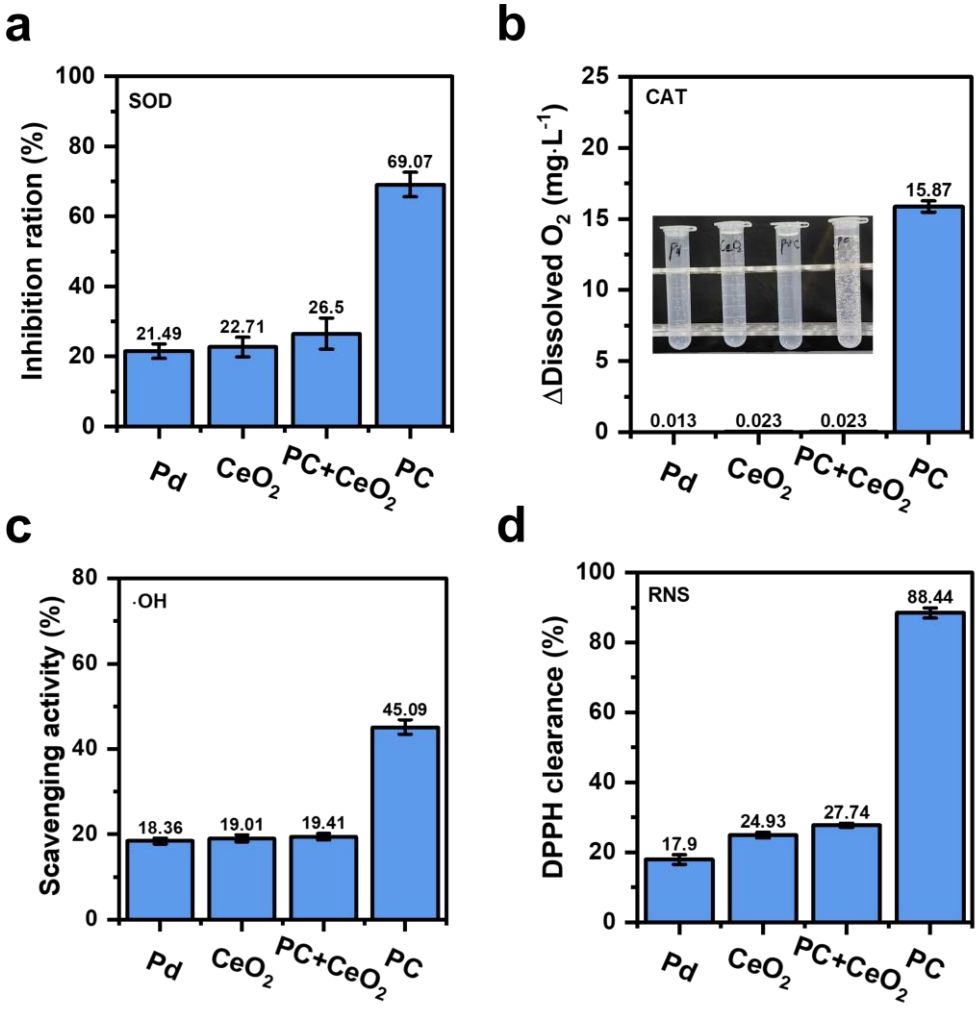

Figure S7. The synergistic effects between Pd and CeO_2 enhanced the antioxidant activities of Pd-CeO_2 (PC). (a) The SOD-like activities of CeO_2 nanoparticles (NPs), Pd nanosheets (NSs), the physical mixing of Pd NSs and CeO_2 NPs (Pd+CeO_2) and Pd-CeO_2 (PC) to scavenge $O_2^{\bullet-}$. (b) The CAT activities of CeO_2 NPs, Pd NSs, Pd+ CeO_2 and PC to generate O_2 (insert showed the corresponding pictures of O_2 generation). (c) •OH scavenging capacities of CeO_2 NPs, Pd NSs, Pd+ CeO_2 and PC that were detected by salicylic acid method. (e) DPPH clearance in the presence of CeO_2 NPs, Pd NSs, Pd+CeO_2 and PC. All tests were performed under physiological conditions (PBS, 0.01M, pH = 7.4), n=3.

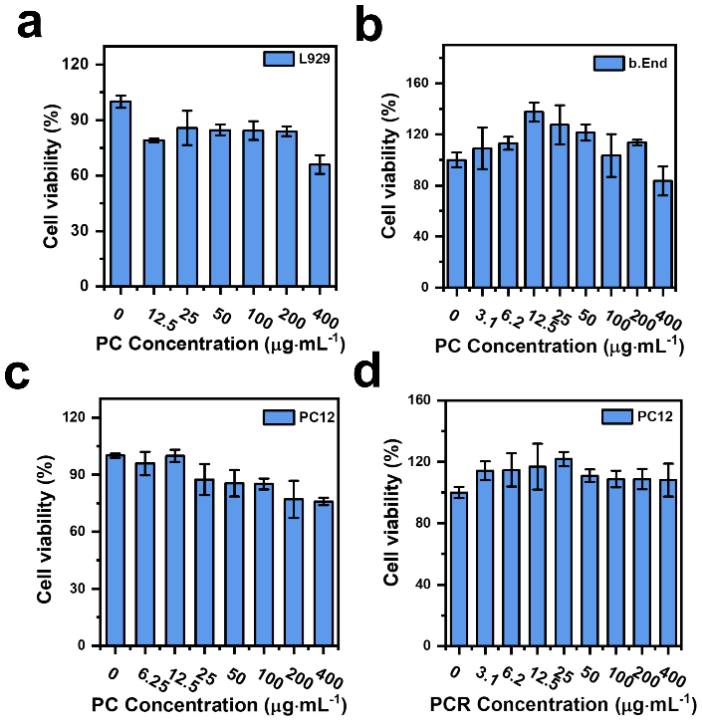

Figure S8. *In vitro* cytotoxicity of PC and PCR nanozymes. Viability measurements of different cells in the presence of PC and PCR nanozymes determined by MTT assay.

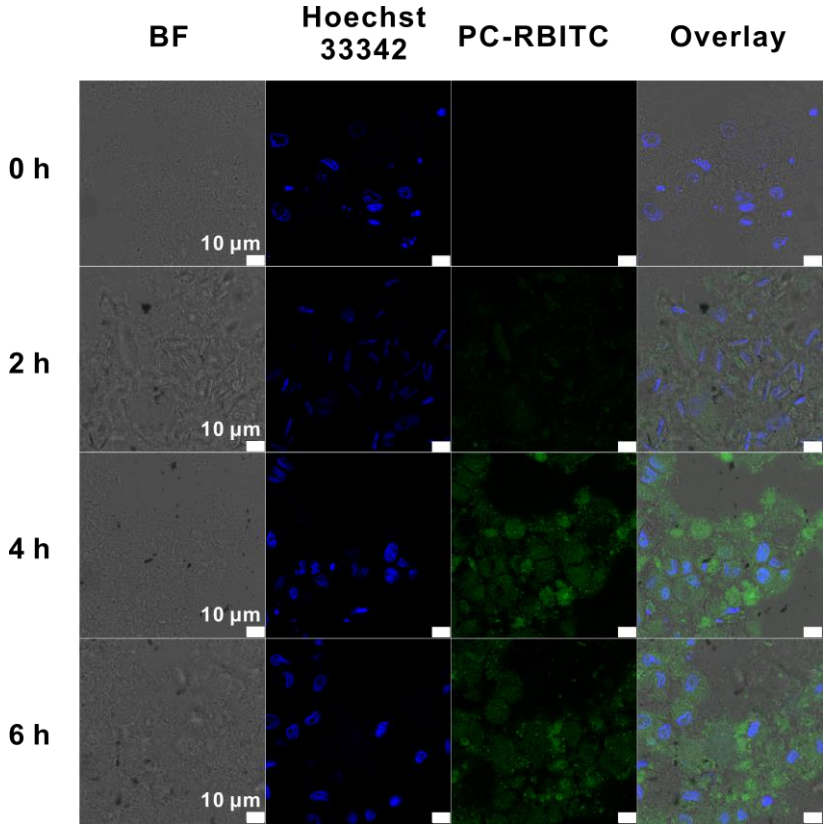

Figure S9. Confocal laser fluorescence microscope (CLFM) images of PC12 cells ingesting PC in different incubation time (Scale bar = 10 μm).

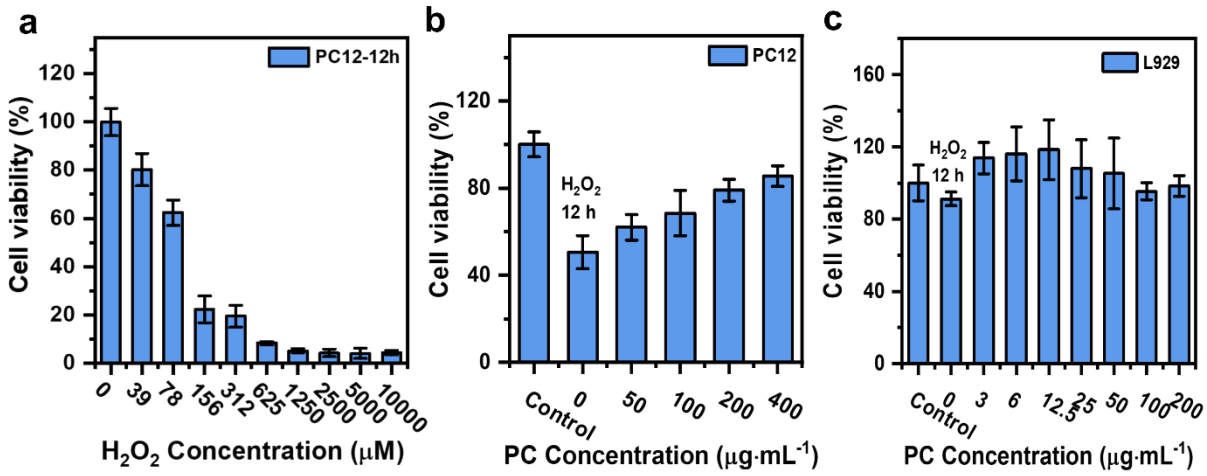

Figure S10. (a) Effects of different concentrations of H_2O_2 on viability of PC12 cells. Viabilities of PC12 (b) and L929 cells (c) that were incubated with H_2O_2 in the presence of PC determined by MTT assay (n=5).

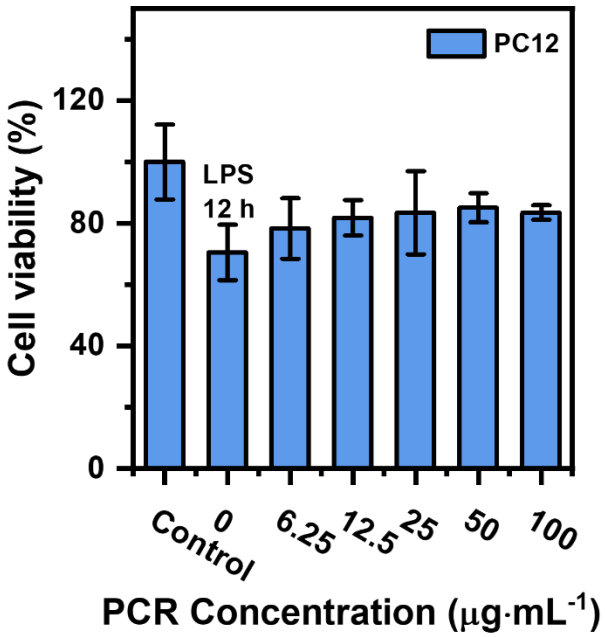

Figure S11. Viability measurement of LPS-treated PC12 cells in the presence of PCR nanozymes determined by MTT assay (n=5).

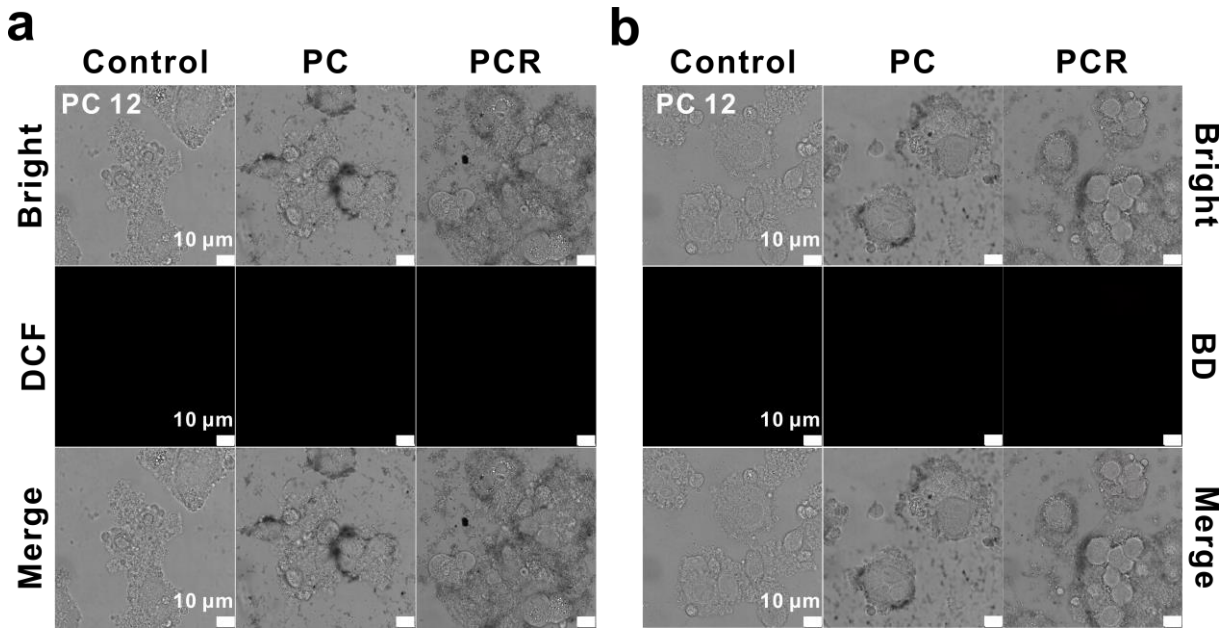

Figure S12. CLFM images of PC12 intracellular ROS (a) and RNS (b) levels under different conditions. Green, DCF fluorescence produced by ROS oxidizing nonfluorescent DCFH. Red, benzotriazole derivatives (BD) fluorescence generated by •NO oxidizing DAF-FM. Scale bar = 10 μm.

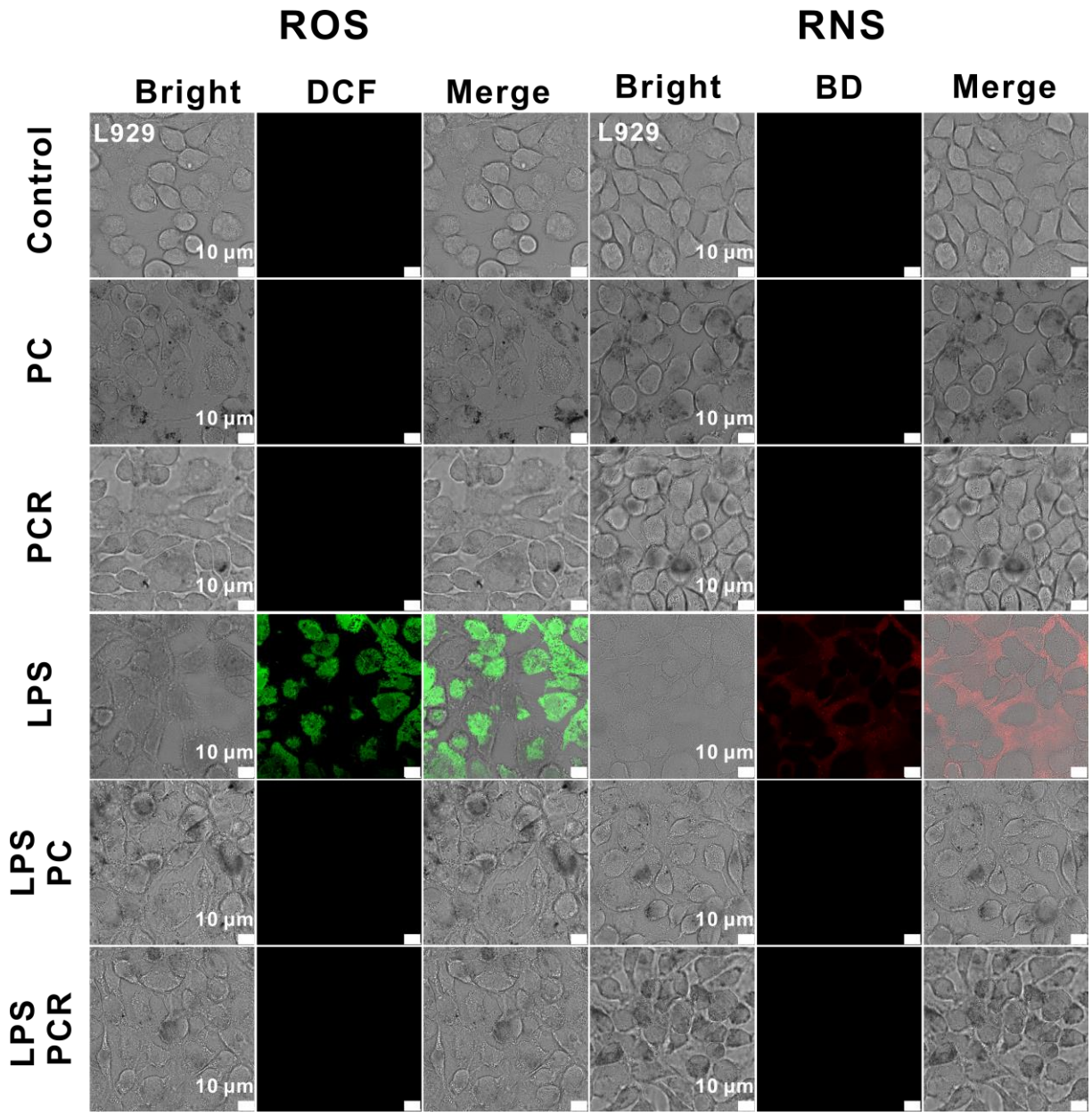

Figure S13. CLFM images of L929 intracellular ROS and RNS levels under different conditions. Green, DCF fluorescence produced by ROS oxidizing nonfluorescent DCFH. Red, benzotriazole derivatives (BD) fluorescence generated by •NO oxidizing DAF-FM. Scale bar = 10 μm.

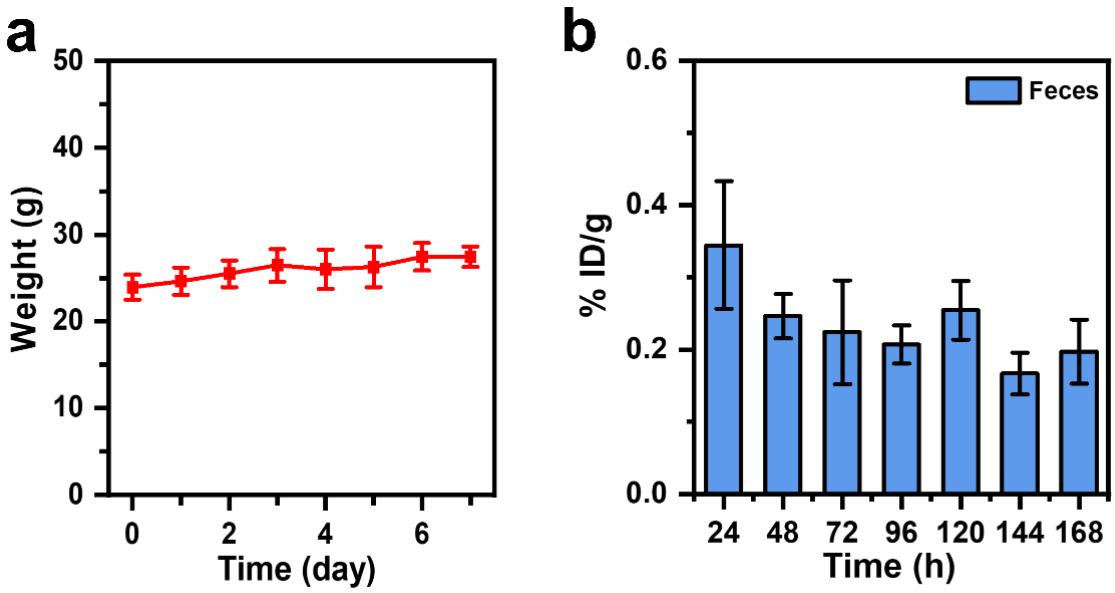

Figure S14. Biosecurity of PCR. (a) Body weight curve of mice injected with PCR nanozymes (n=3). (b) Feces excretions of PCR nanozymes (n=3). %ID/g = percentage of the injected dose per gram of weight.

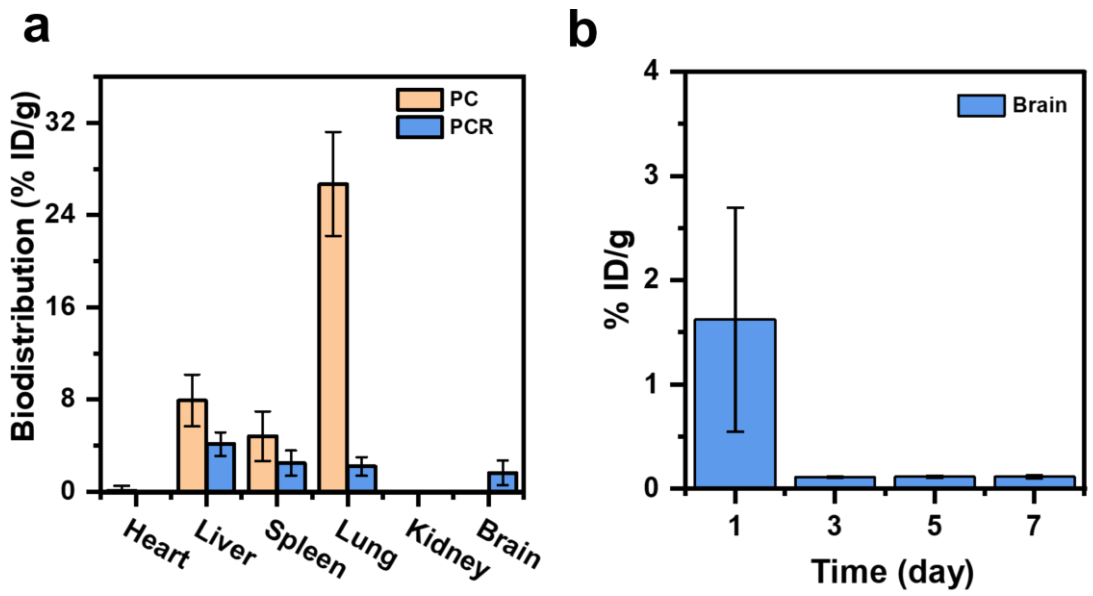

Figure S15. (a) Biodistribution of PC and PCR nanozymes in main organs at 1 day post injection (n=3). (b) Biodistribution of PCR nanozymes in brain at 1, 3, 5 and 7 day post injection (n=3). %ID/g = percentage of the injected dose per gram of weight.

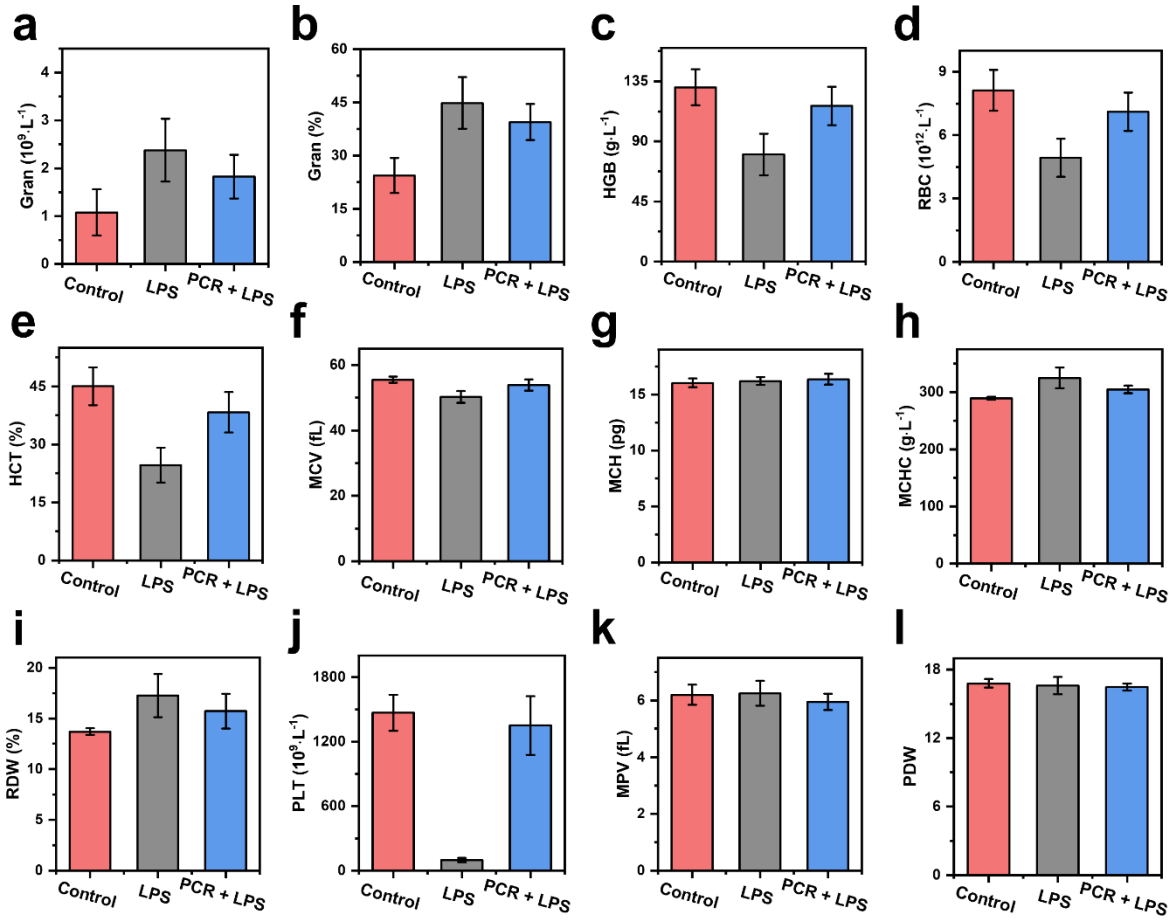

Figure S16. Blood routine data of LPS-injected mice with or without PCR nanozymes treatment. All data were collected after final treatment (n=6).

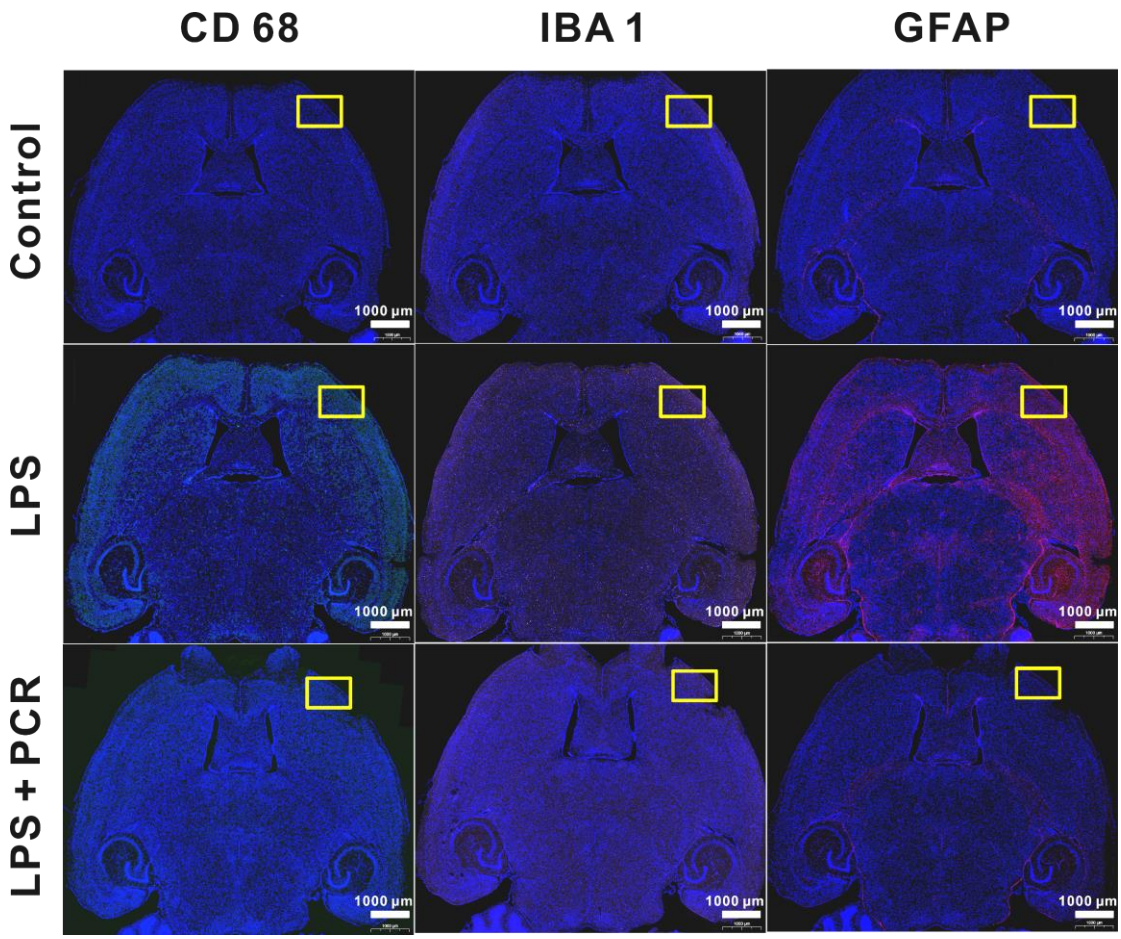

Figure S17. Representative immunohistochemical images of brain sections stained with antibody to CD68, antibody to IBA 1 and antibody to GFAP. CD68, green; IBA1, pink; GFAP, red; DAPI, blue. Scale bar = 1000 µm.

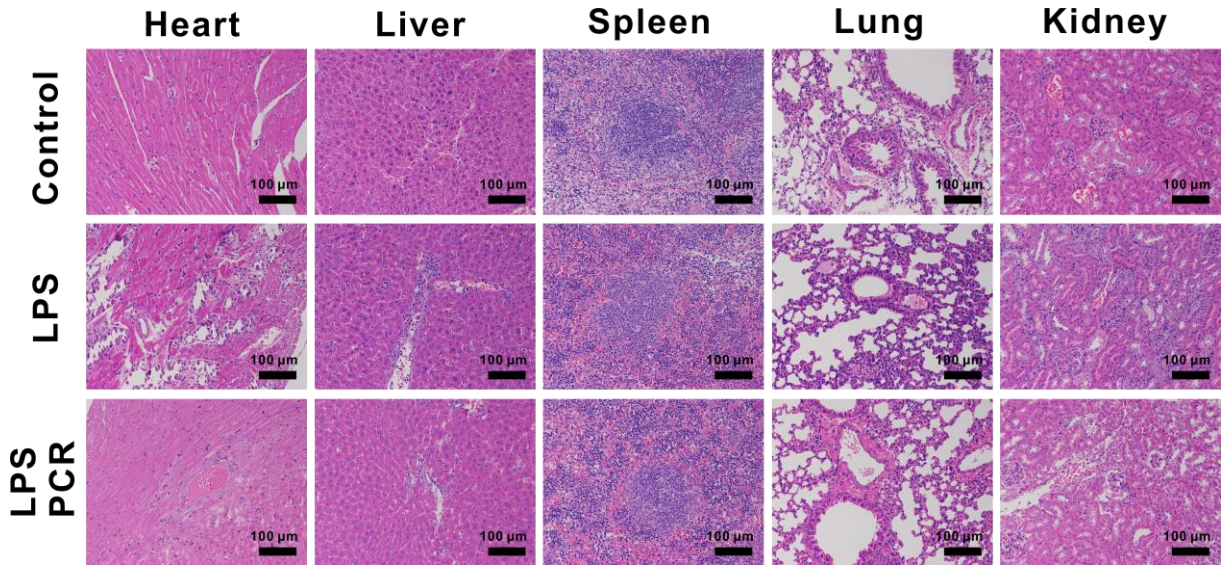

Figure S18. The H&E stain sections of some major organs (heart, liver, spleen, lung and kidney) in different groups. (Scale bar = 100 μm)

Table S1. The kinetic parameters of CAT-like activity in PC and previously reported catalytic nanomaterials.

Catalyst	Substrate	Km [mM]	Vmax [mg*L^{-1}*min^{-1}]
Pd@Ir[1]	H_2O_2	137.36	1.196×10^{-3}
Catalase[2]	H_2O_2	54.3	31.1
Pd NSs[3]	H_2O_2	164.83	2.12
Pd-Ru NSs[3]	H_2O_2	31.02	8.43
PC	H_2O_2	20.38	156.19
Ti_3C_2/CeO_2-PVP[4]	H_2O_2	60.8	0.39
Au@CeO_2[5]	H_2O_2	30.25	0.05

Reference

1. Z. Ye, Y. Fan, T. Zhu, D. Cao, X. Hu, S. Xiang, J. Li, Z. Guo, X. Chen, K. Tan, N. Zheng, *ACS Applied Materials & Interfaces*, 2022, ***14,*** 23194.
2. J. Mu, L. Zhang, M. Zhao, Y. Wang, *Journal of Molecular Catalysis A: Chemical*, 2013, ***378,*** 30.
3. J. Ming, T. Zhu, J. Li, Z. Ye, C. Shi, Z. Guo, J. Wang, X. Chen, N. Zheng, *Small*, 2021, ***17,*** 2103645.
4. M. Tang, Y. Shi, L. Lu, J. Li, Z. Zhang, J. Ni, W, Wang, Y. Zhang, T. Sun, Z. Wu, *Chemical Engineering Journal*, 2022, ***449,*** 137847.
5. W. Sheng, X. Wu, M. Fu, C. Chen, Z. Bai, M. Xing, C. Zhang, L. Chong, J. Li, F. Gao, *Chemical Engineering Journal*, 2023, ***470,*** 144359.